Chemistry – A European Journal

ChemEurJ Chemistry Europe European Chemical Societies Publishing

RESEARCH ARTICLE OPEN ACCESS

A Cyclic $\{Ni^{II}_8Dy^{III}_4\}$ Cluster Where the Dy^{III} Moments Are Organized by the Transition Metal Spins

Imon J. Dutta[1] | Kartik Chandra Mondal[2,3] | Jonas Braun[3,4,5] | Wolfgang Wernsdorfer[5,6] | Christopher E. Anson[3] | Yanhua Lan[3] | Kuduva R. Vignesh[1] | Annie K. Powell[3,4,5]

[1]Department of Chemical Sciences, Indian Institute of Science Education and Research (IISER) Mohali, Mohali, Punjab, India | [2]Department of Chemistry, Indian Institute of Technology Madras, Chennai, India | [3]Institute of Inorganic Chemistry, Karlsruhe Institute of Technology (KIT), Karlsruhe, Germany | [4]Institute of Nanotechnology, Karlsruhe Institute of Technology (KIT), Karlsruhe, Germany | [5]Institute for Quantum Materials and Technologies, Karlsruhe Institute of Technology (KIT), Karlsruhe, Germany | [6]Physikalisches Institut, Karlsruhe Institute of Technology (KIT), Karlsruhe, Germany

Correspondence: Kartik Chandra Mondal (csdkartik@iitm.ac.in) | Kuduva R. Vignesh (vigneshkuduvar@iisermohali.ac.in) | Annie K. Powell (annie.powell@kit.edu)

Received: 26 May 2026 | **Revised:** 11 July 2026 | **Accepted:** 15 July 2026

Keywords: 3d–4f complex | *ab initio* calculations | coordination chemistry | MicroSQUID | single molecule magnets

ABSTRACT

A series of $[Ni_8Ln_4(CO_3)_4(L)_8(NO_3)_2(H_2O)_8\ (MeOH)_4](NO_3)_2$ (Ln = Dy (**1**), Gd (**2**), Y (**3**)) cyclic coordination clusters containing four carbonate bridges were isolated and studied using SQUID and microSQUID experiments and quantum mechanical calculations. The dodecanuclear Ni_8Dy_4 complex exhibits slow relaxation of the magnetization confirmed by the presence of temperature- and field-dependent magnetic hysteresis loops. The competing interactions and the anisotropic nature within the cluster were analyzed using DFT and ab initio calculations and revealed that the spin structure of the Dy^{III} ions is steered by the interactions mediated through the Ni^{II} ions.

1 | Introduction

Organization of spins in homometallic Dy^{III} clusters can lead to various magnetic effects such as single-molecule magnetism (single-molecule magnets—SMMs) or toroidicity (single molecule toroics—SMTs). The spin structures in such compounds are generally driven by dipolar couplings between Dy^{III} centers [1–4]. However, in heterometallic 3d–4f systems, the situation can be more complicated, particularly in cases where the Dy^{III} ions are too far apart for direct dipolar Dy–Dy coupling to be significant. Here, the coupling of the spins of the intervening 3d ions with the Dy^{III} ions can organise the Dy^{III} moments to give exotic spin structures. Particularly, when these anisotropic Dy^{III} ions are coupled with anisotropic 3d transition metal ions such as Fe^{II}, Co^{II}, Ni^{II} and Mn^{III}, they exhibit substantial zero-field splitting (D); this results in strongly coupled spin systems. This has, for example, been shown in an Fe_8Dy_{12} SMM [5] as well as an $Fe_{18}Dy_6$ SMT [6] and also in Fe_8Dy_8 [7], Mn_8Dy_8 [8], and Cr_8Dy_8 [9] wheels. Ni^{II} has been less frequently used as the 3d heterometal in 3d–4f clusters. Though the majority of Ni^{II} complexes have D values falling within the −200 to +200 cm^{-1} range [10, 11], which is usually observed for mononuclear Fe^{II} and Co^{II} complexes, a few Ni^{II} complexes possess a D value over −400 cm^{-1} [12–14]. For example, a trigonal bipyramidal Ni^{II} complex shows a D value of ≈ −535 cm^{-1} due to the lack of axial symmetry breaking [15, 16]. Therefore, the selection of Ni^{II} as the 3d metal is motivated by its substantial magnetic anisotropy, which arises from second-order perturbative mixing

Dedicated to Prof. Hansgeorg Schnöckel on the occasion of his 85th birthday.

Imon J. Dutta and Kartik Chandra Mondal are contributed equally to this work.

of excited states and leads to pronounced D [10, 15, 17, 18]. Ni^{II}–Ln^{III} complexes are attractive because they combine the large magnetic anisotropy of Ln^{III} ions with the ability of Ni^{II} to mediate appreciable exchange coupling [17]. Moreover, promising observations such as the identification of ferromagnetic coupling between Ni^{II}–Ln^{III} ions suggest a beneficial synergy within 3d–4f complexes, significantly reduces the QTM and offering great potential SMMs with long relaxation times (>100 s) [19–24]. Examples where it has been used include Ni_2Dy_2 [25], Ni_3Dy_3 [26], Ni_4Dy_2 [27], $Ni_{10}Ln_5$ [28], and $Ni_{22}Gd_{44}$ [29] clusters.

Here we report a cyclic dodecanuclear heterometallic $\{Ni_8Dy_4\}$ complex $[Ni_8Dy_4(CO_3)_4(L)_8(NO_3)_2(H_2O)_8(MeOH)_4](NO_3)_2{\cdot}5MeOH{\cdot}4H_2O$ (**1**) obtained from a methanolic solution of Dy^{III}:Ni^{II}:H_2L:Et_3N in a yield of 30%–40% (H_2L = (E)-2-(2-hydroxy-3-methoxybenzylideneamino)phenol). The Gd^{III} (**2**) and Y^{III} (**3**) analogs were also synthesized using the same synthetic procedure. The magnetic SQUID and microSQUID data of these three isostructural compounds are described and rationalized by *ab initio* CASSCF and DFT calculations. Furthermore, the role of dipolar coupling in this large heterometallic $\{Ni^{II}{}_8Dy^{III}{}_4\}$ cluster has been verified with DFT/PHI calculations. The important role of dipolar coupling in lanthanide-containing clusters [30, 31] and in the lanthanide radical system has been explored [32]. In lanthanide radical complexes, the exchange coupling between a lanthanide ion and an organic radical is frequently stronger than the exchange between two lanthanide centers. These lanthanide-radical exchange interactions are also comparable to typical 3d-lanthanide exchange interactions. Therefore, we thoroughly calculate dipolar contributions for all relevant metal-metal pairs (Ni–Dy and Ni–Ni) and compare these terms with the exchange parameters. This study highlights the crucial role of dipolar interactions in accurately reproducing the experimental dc magnetic data and in determining the SMM properties.

2 | Results and Discussion

2.1 | Crystallography

Compound **1** crystallizes in the tetragonal space group $P\bar{4}2_1c$ with $Z = 2$, and the $[Ni_8Dy_4(\mu_5\text{-}CO_3)_4(L)_8(MeOH)_4(NO_3)(OH_2)_{10}]^{3+}$ cluster molecule occupies a site with crystallographic $\bar{4}$ site symmetry (Tables S1 and S2). The asymmetric unit of the cluster and a view of the complete molecule are shown in Figure 1, with two views of the cluster core in Figure 2.

The core of the cluster can be considered to be made up of four nonlinear Dy-Ni-Ni subunits, arranged alternately above and below the Ni_8Dy_4 mean plane, resulting in a highly nonplanar cyclic system. The organic ligands $(L)^{2-}$ are the doubly deprotonated forms of the Schiff base formed between *o*-vanillin and 2-aminophenol, and as expected, the Ni^{II} ions occupy Pocket I of the ligand, made up of the two phenoxido oxygens and the imino nitrogen, whereas the methoxido group and phenoxido oxygen of the vanillin (Pocket II) chelate a Dy^{III}. Each pair of adjacent Ni^{II} in the cycle is then bridged by two oxygens from aminophenol sub-units, giving the bridging coordination mode shown in Scheme 1. Additional linkages between the metal centers in the ring are provided by the four carbonate bridges, each of which coordinates to three Ni^{II} and two Dy^{III} (Scheme 1,

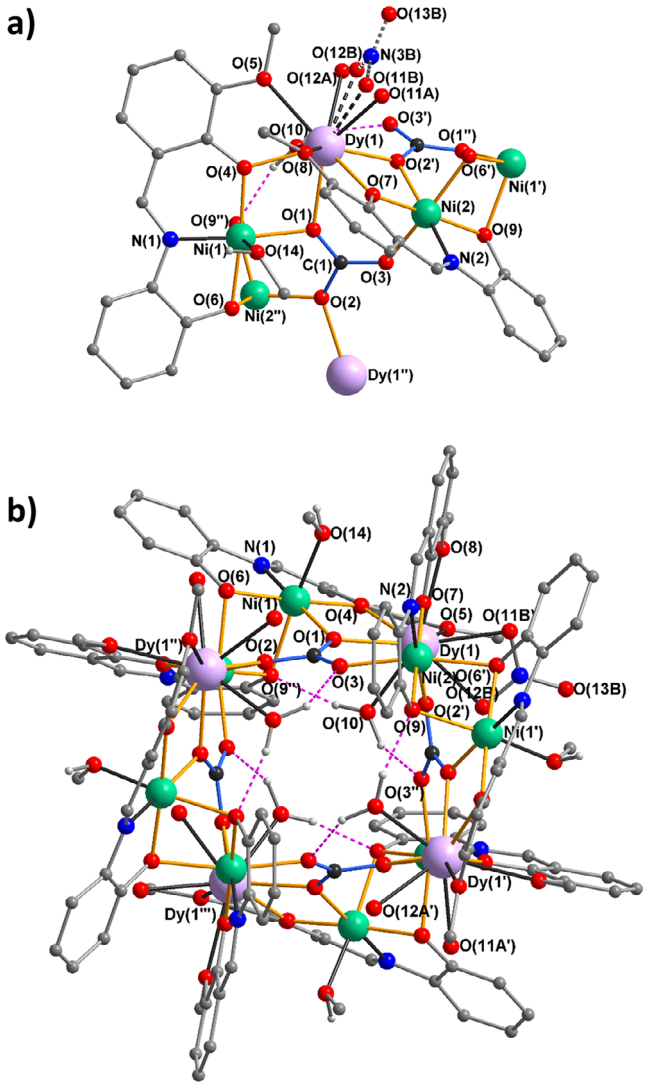

FIGURE 1 | (a) Asymmetric unit of the $[Ni_8Dy_4(\mu_5\text{-}CO_3)_4(L)_8(MeOH)_4(NO_3)(OH_2)_{10}]^{3+}$ cluster in **1**, showing the connections to symmetry-equivalent metal atoms. For the disordered ligands on Dy1, the minor (25%) nitrate is shown with dashed bonds; the corresponding water ligands (occupancy 75%), O(11A), and O(12A), are shown with solid Dy—O bonds. (b) View of the complete cluster molecule viewed down the crystal *c*-axis, with the disordered nitrate ligand shown in one of its four possible positions (chelating Dy(1) at the top right of the molecule as shown). Dy violet, Ni green, O red, N blue, C grey, and organic H-atoms omitted for clarity. Hydrogen bonds shown as purple dashed lines; carbonate C—O bonds emphasized in light blue. Primed atoms at $\{y, -x, 1-z\}$, double-primed atoms at $\{-y, x, 1-z\}$, and triple-primed atoms at $\{-x, -y, z\}$.

Figure 2). Further intramolecular stabilization is provided by the four water ligands O(10), which each make a hydrogen bond to a phenoxido oxygen and an oxygen of a carbonate bridge.

Peripheral coordination for the four Dy^{III} is provided by either a chelating nitrate (on one Dy^{III}) or two further water ligands (the other three Dy^{III}). There is no ordering of the molecules in the crystal in terms of the orientation of the single nitrate ligand, resulting in the apparent $\bar{4}$ site symmetry of the cluster. This fourfold symmetry results from the averaging of the coordination

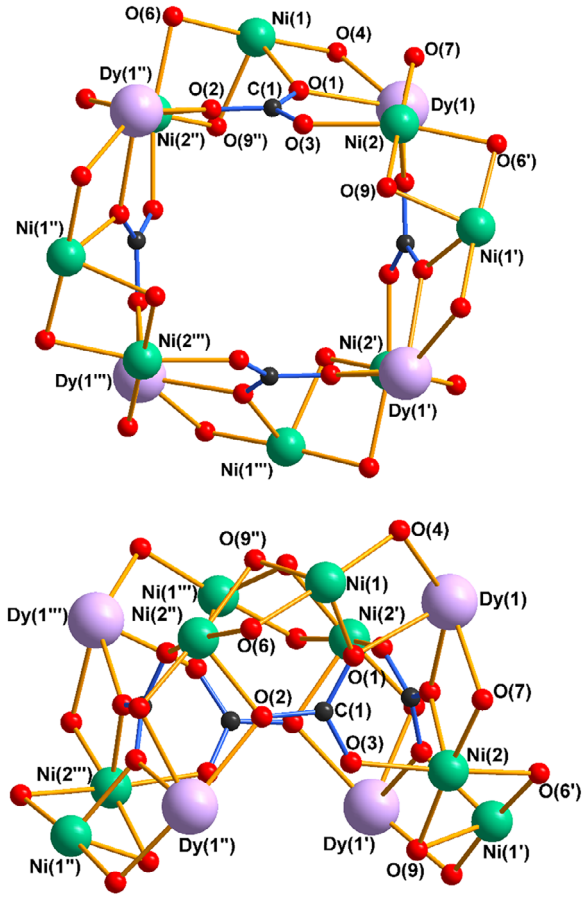

FIGURE 2 | Two views of the Ni_8Dy_4 core in **1**, showing the carbonate and phenoxide bridges between the metal atoms. Atom colors and symmetry codes as for Figure 1.

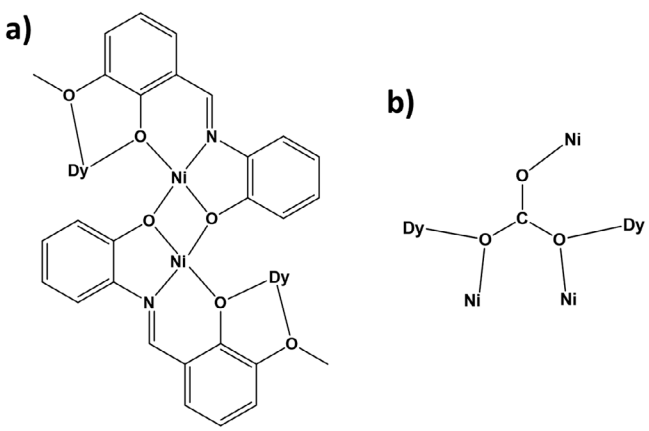

SCHEME 1 | **(a)** Coordination mode of two of the ligands $(L)^{2-}$ on either side of a Ni_2 dinuclear unit within the Ni_8Dy_4 cluster in **1**. (b) Bridging mode of the $(\mu_5{-}CO_3)^{2-}$.

environments of the four Dy centers over the crystal as a whole. This means that in the asymmetric unit there is a 25:75 disordered superposition (Figure 1a). The coordination sphere of Ni(1), on the other hand, is completed by an ordered methanol ligand.

Overall, the cluster is thus a trication, and this charge is balanced by three lattice nitrates. Two of these are provided by the nitrate centered on the atom N(41), which occupies a site of twofold symmetry (thus two nitrates per cluster), whereas the third nitrate is disordered over the other $\bar{4}$ site in the structure. The primary intermolecular linkage involves the methanol ligands on four of the Ni^{II} centers, which form hydrogen bonds to the oxygen O(41) of the nitrate on the twofold site. This hydrogen bonding thus links each cluster to four other symmetry-related clusters at $\{-x, 1-y, z\}$, $\{1-y, x, 1-z\}$, $\{x, -1+y, z\}$, and $\{-1+y, -x, 1-z\}$, resulting in undulating "chessboard" sheets parallel to [001]. The space group $P\,\bar{4}2_1c$ is non-centrosymmetric, and the essentially zero Flack χ parameter (−0.037(4)) shows the absence of any twinning of the structure by inversion.

Such incorporation of CO_3^{2-} derived from atmospheric CO_2 has also been observed in several Ni^{II} [33], Dy_6 [34], Ln_{10} [35], $NaNi_5La_4$, and $Ni_{30}La_{20}$ [36] complexes. It is worth noting that when the same reaction was performed under inert atmosphere, it resulted in completely different products [25].

In terms of magnetic coupling, considering the molecular structure of complex **1**, the following can be expected. Ni—Ni interactions within each dimeric Ni^{II}_2 unit are expected to be ferromagnetic since the Ni-phenoxide-Ni angle of 88.13°(1) is smaller than the suggested critical angle of 96° [37]. The Ni—O—Dy bridging angle is equal to 103.46° in complex **1**. Furthermore, Ni_2Dy_2 sub-units of **1** are also further magnetically coupled to alike neighboring units by additional *syn-anti/anti-anti* bridging modes (Figure S1c) of CO_3^{2-} which are reported to mediate weak antiferromagnetic interactions [33, 36]. Each cationic molecular unit of **1** is involved in intermolecular H-bonding, which could additionally mediate weak antiferromagnetic interactions (Figure S2).

2.2 | Experimental Magnetic SQUID Data

The χT values at room temperature are 65.93 cm^3 K mol^{-1} for **1**, 40.65 cm^3 K mol^{-1} for **2**, and 8.36 cm^3 K mol^{-1} for **3**, and are in good agreement with the expected values for compounds made of eight Ni^{II} ions ($S = 1$, $g = 2.1$, $C = 1.10$ cm^3 K mol^{-1}) and four Dy^{III} ions ($S = 5/2$, $L = 5$, $^6H_{15/2}$, $g = 4/3$, $C = 14.17$ cm^3 K mol^{-1}), four Gd^{III} ions ($S = 7/2$, $L = 0$, $^8S_{7/2}$, $g = 2$, $C = 7.88$ cm^3 K mol^{-1}), of 65.48, 40.3, and 8.8 cm^3 K mol^{-1}, respectively. The χT product for **1** remains essentially constant from room temperature to 100 K, below which it decreases slowly, followed by a sharp drop to 17.51 cm^3 K mol^{-1} at 1.8 K (Figure 3, top). The χT versus T plots of **2** and **3** follow a similar profile with a gradual increase down to 100 K, below which the χT product of **2** increases more rapidly, reaching a maximum of 44.6 cm^3 K mol^{-1} at 11 K, then sharply decreasing to 31.7 cm^3 K mol^{-1} at 1.8 K. This is indicative of the presence of a dominant ferromagnetic exchange interaction (Figure 3, bottom). For **3,** the gradual increase continues down to 55 K and then sharply decreases to 0.78 cm^3 K mol^{-1} at 1.8 K (Figure 3, bottom).

The magnetization curves of **1** increase rapidly on increasing the dc magnetic field (H) below 1 T, above which M linearly increases up to 7 T to reach a maximum value of 30.31 μ_B (**1**) at 2 K (Figure S3). The M versus H/T plots (Figure S3, inset) for **1** do not superpose on a single master curve at different temperatures, indicating the presence of low-lying energy states

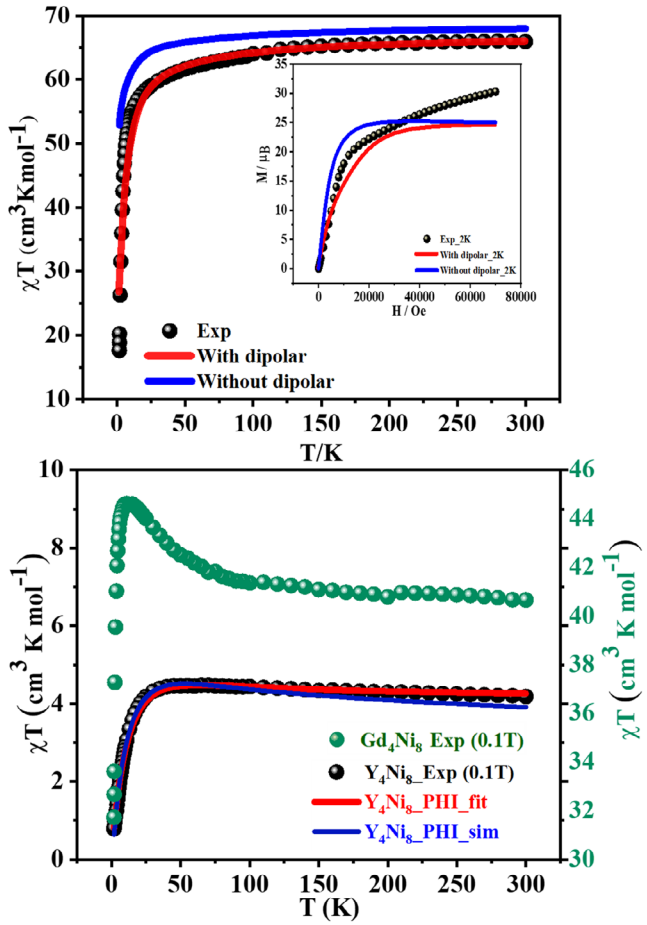

FIGURE 3 | The χT vs. T and M vs. H at 2 K (inset) plots of complex **1** (top). The χT vs. T plot of complexes **2** and **3** (bottom). The curves for **3** obtained from the PHI fitting and simulated using the parameters from the DFT calculations are shown as red and blue lines, respectively.

and/or anisotropy in the system [25, 38–43]. The magnetization of **2** behaves similarly, reaching a maximum value of 37.7 μ_B at 2 K (Figure S4). This would be consistent with a spin state of $S = 19$ to 22. The magnetization of **3** increases almost linearly up to 7 T to reach a maximum value of 8.6 μ_B at 2 K (Figure S4).

The temperature-dependent ac susceptibility measurements on complex **1** reveal the presence of in-phase (χ') and weak out-of-phase (χ'') signals below 4 K (Figure S5), indicating slow relaxation of magnetization. Given the weakness of the signal at zero applied dc field, additional χ' and χ'' versus frequency (Figure S6) measurements were performed under the optimal field of 2 kOe. This leads to the observation of maxima in the χ'' versus frequency plots (Figure S6, right) at lower frequencies (Figures S6–S8).

The temperature dependence of the relaxation times, extracted from these data using a generalized Debye model, was fitted using Equation 1.

$$\tau^{-1} = A \cdot T + \tau_0^{-1} \cdot \exp\left(-\frac{U_{\text{eff}}}{k_B T}\right) \quad (1)$$

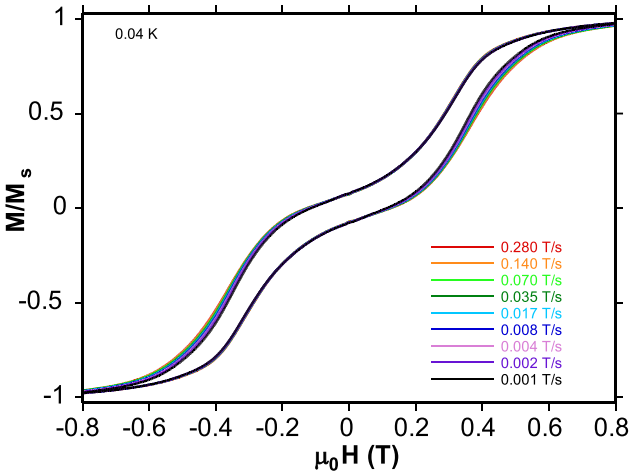

FIGURE 4 | The sweep rate-dependent hysteresis loops of **1** at 0.04 K.

Although the relaxation times can be fitted using only an Orbach process within the experimental error, this leads to a rather slow relaxation rate of $\tau_0 = 1.4 \cdot 10^{-6}$ s. The inclusion of an additional direct process, the consequence of the applied dc field of 2 kOe, improves the fit significantly, resulting in a typical Orbach relaxation rate of $\tau_0 = 2.4 \cdot 10^{-8}$ s and an effective energy barrier of 18.3 K.

2.3 | MicroSQUID Measurements

MicroSQUID measurements [44] were performed on single crystals of complex **1** at temperatures between 0.04 and 0.8 K and sweep rates between 0.001 and 0.280 T/s. Sweep rate-independent hysteresis loops at 0.04 K show a coercive field of 0.6 T at a sweep rate of 0.28 T/s (Figures 4 and S9). A correlation between the spin structure and the observed magnetization behavior at 40 mK is provided after the results of the quantum chemical calculations in terms of coupling constants and the relative orientation of the Ni^{II} and Dy^{III} spins.

2.4 | Quantum Chemical Calculations

In order to assess the magnetic properties of the Ni_8Ln_4 compounds, the Y-analogue (**3**) is considered first to quantify the Ni^{II}–Ni^{II} interactions. The possible exchange pathways in **3** as well as in **1** and **2** are shown in Figure S11. For this, the dc magnetic data of **3** were fitted using PHI [45] resulting in a Ni–Ni intradimer interaction (J_2) of +9.1 cm^{-1} and an interdimer interaction (J_3) of −2.36 cm^{-1}. Note that here and elsewhere in this paper we use a spin Hamiltonian of the $H = -2J(\mathbf{S_1} \cdot \mathbf{S_2})$ formalism. This is in good qualitative agreement with the results of DFT calculations, which gave coupling constants of J_2 as +13.2 cm^{-1} and J_3 as −4.4 cm^{-1}, respectively. The PHI fitted values are slightly smaller than DFT values; such an overestimation/underestimation is common with DFT-computed and PHI-fitted J values [46–50]. We noted earlier that J_2 was expected to be ferromagnetic since the Ni—O—Ni angles at O(6) and O(9) are both less than 90° [37]. The χT versus T plot from the PHI fitting and that simulated by PHI using the coupling constants obtained from the DFT calculations are each shown as solid lines in Figure 3 bottom. This results in a ground

state with $S = 0$, as shown by the DFT calculated spin density plots in Figure S10 (BS2).

We then considered the Gd-analogue (**2**), which contains paramagnetic and isotropic lanthanide ions. This offers the opportunity to investigate the Ni–Ln coupling without interfering anisotropy, making DFT calculations possible. The different spin configurations in **2** are shown in Figure S11 (top) and Table S4, respectively. For **2**, DFT calculations yielded the Gd^{III}–Ni^{II} exchange interaction (J_1) as +0.54 cm^{-1}, while the intra (J_2) and interdimer (J_3) Ni^{II}–Ni^{II} exchange interactions are similar to those for **1** with +13.4 and −4.41 cm^{-1}, respectively. A previous magneto–structural correlation for {GdNi} and {NiGdNi} complexes showed that Gd—O—Ni angles larger than 84° result in ferromagnetic interactions; with Gd—O—Ni angles of 91°, 96°, and 107° associated with Ni–Gd couplings of +0.18, +0.30, and +1.07 cm^{-1}, respectively [20]. The Gd—O—Ni angle found here, 103.5°, and the computed J_1 of +0.54 cm^{-1} are consistent with this trend. The DFT-computed spin–density plots of **2** in Figure S12 indicate a ferromagnetic spin ground state of $S = 22$ for the {NiGd} cyclic structure, highlighting its significant high-spin character among hetero metallic {NiGd} cyclic assemblies [29, 51–57].

We are now in a position to assess the magnetic behavior of the Dy-analogue (**1**). For this, we carried out *ab initio* CASSCF/RASSI-SO/SINGLE_ANISO calculations using the MOLCAS 8.2 [58] program. The orientation of the anisotropy g_{zz} axes in the ground doublets of the Dy^{III} ions and the D_{zz} axes in the Ni^{II} ions is depicted in Figure 5.

This arrangement of axes in the ground state also allows for the rationalization of the micro-SQUID measurements (Figure 4). At zero field, all Ni^{II} moments are essentially parallel to the four-fold axis, whereas the Dy^{III} moments have major components pointing along the opposite direction of the four-fold axis. This results in a net magnetic moment aided by the single-ion anisotropy of the Dy^{III} ions, leading to open hysteresis. At 0.3 T, an inflection point is observed indicative of a level crossing, which here signals the flipping of the Dy^{III} spins as the magnetic field overcomes the antiferromagnetic Dy–Ni interactions, leading to a steeper increase in magnetization.

To compute the magnetic relaxation of each Dy^{III} and Ni^{II} metal center, we have fragmented complex **1,** considering its extremely large size. The modelled structures are shown in Figure S13. The electronic structure of all four Dy^{III} ions shows that the g tensors in the ground KDs have smaller g_z values than the value of 20 for a pure $m_J = \pm 15/2$ state and large transverse g_x and g_y components (Tables 1 and S5). The presence of transverse components indicates that the ground KDs contain highly mixed m_J states, which is likely to result in efficient QTM.

To investigate the magnetic relaxation of individual Dy^{III} ions, energies of low-lying KD states were computed. Tables 1 and S6 list the computed energy gaps between the ground KDs and the excited states for each Dy^{III} ion. The energy gaps to the first excited KDs are 45.8, 36.0, 36.1, and 36.7 cm^{-1} for Dy1-4, respectively. This reflects the molecular structure with the nitrate localized on Dy1, leading to a larger energy separation between ground and first excited KD but a smaller g_z component in the ground state compared to the other Dy^{III} ions (Tables 1 and S5 and S6).

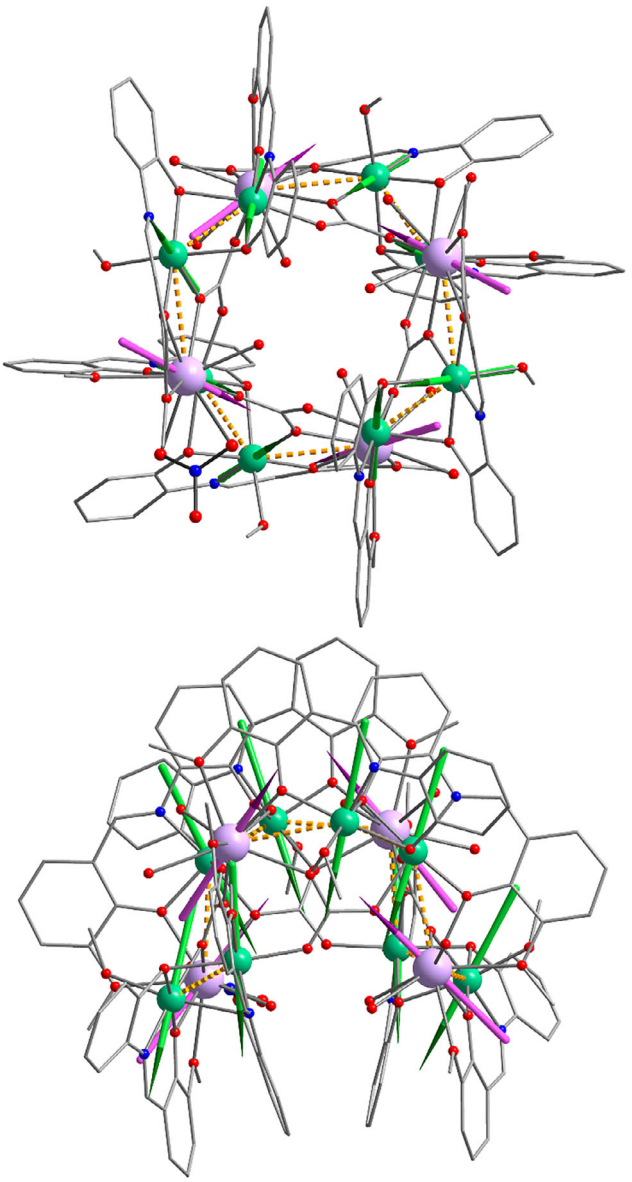

FIGURE 5 | Two views on the anisotropy axes of both Dy^{III} and Ni^{II} ions as computed using SINGLE_ANISO calculations.

Figures 6 and S14 depict a qualitative magnetic relaxation mechanism for Dy1, Dy2, Dy3 and Dy4, respectively. Significant QTM is observed between the ground KDs for the Dy centers, indicating that magnetic relaxation is likely to occur via ground KDs. The presence of QTM in the ground KDs is attributed to the mixing of ±15/2 and ±11/2 states for the Dy1 center and of the ±15/2 and ±3/2 states for Dy2, Dy3, and Dy4 centers. The existence of large QTM in the ground KDs is further validated by computing the crystal-field parameters using SINGLE_ANISO [58], which results in larger non-axial terms ($q \neq 0$ and $k = 2, 4, 6$) compared to the axial terms ($q = 0$ and $k = 2, 4, 6$) (Table S7) [59]. This suggests that negligible slow magnetization relaxation is expected from the individual Dy ions. However, when the Dy ions are coupled with anisotropic Ni ions, the reorientation of magnetization with reasonable barriers is possible. Therefore, the anisotropic nature

TABLE 1 | Low-lying energies (cm^{-1}) and g-tensors of the Dy^{III} fragments that originate from the corresponding ground Kramers Doublets (KDs).

KD	Dy1	Dy2	Dy3	Dy4
1	0.0	0.0	0.0	0.0
2	45.8	36.0	36.1	36.7
3	139.8	127.7	127.8	128.4
4	213.3	178.7	178.7	179.7
5	283.0	226.6	226.6	228.0
6	379.5	299.9	299.9	301.6
7	467.4	366.6	366.7	368.5
8	570.4	401.2	401.2	403.4
Ground state KDs				
g_x	0.4498	0.4427	0.4431	0.4332
g_y	1.9698	1.8436	1.8491	1.7874
g_z	16.9691	18.2526	18.2910	18.3448

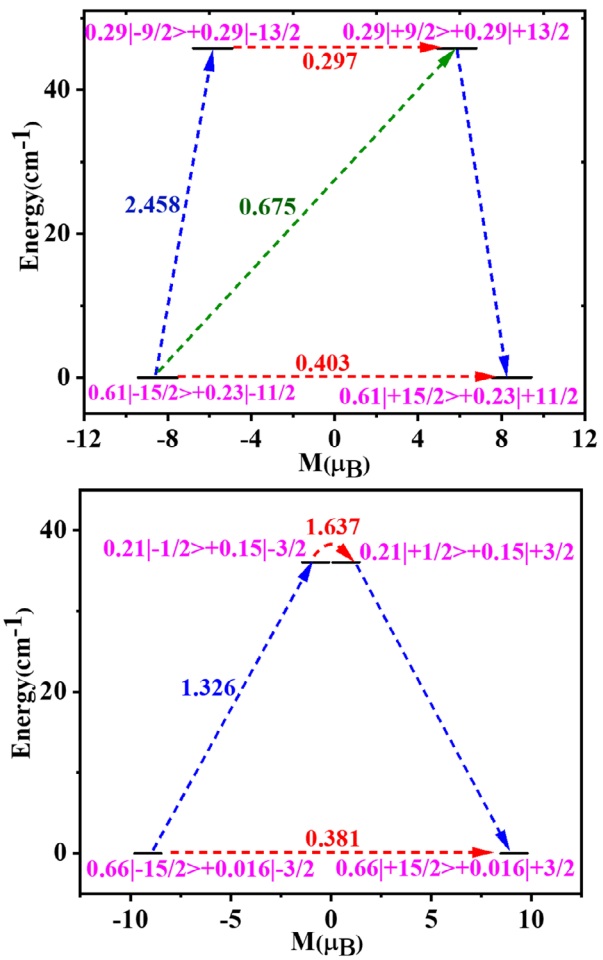

FIGURE 6 | Magnetization blocking barrier for Dy1 (above) and Dy2 (below) in **1**. The barriers for Dy3 and Dy4 are similar to that for Dy2. The black lines indicate the Kramers doublets (KDs). The blue and green arrows show the possible pathway through Orbach and Raman relaxation, respectively. The dotted red lines represent QTM/TA-QTM. The numbers provided at each arrow are the mean absolute values for the corresponding matrix element of the transition magnetic moment.

of Ni ions was verified by computing their axial ZFS values and calculating the exchange interactions between the metal centers.

The possible QTM arising from each Dy^{III} ion may be suppressed if (i) the Ni^{II} ions exhibit significant anisotropy and (ii) there are substantial magnetic exchange interactions between the Dy^{III} ions and the Ni^{II} ion. To elucidate the impact of the anisotropic behavior of Ni^{II} ions and the exchange interactions on the SMM characteristics of complex **1**, we computed the *D* value of the Ni^{II} ion utilizing the SINGLE_ANISO method and the Dy···Ni exchange interactions employing POLY_ANISO. Our computations predict the *D* values for the Ni^{II} ions in the range of −12.4 to +9.5 cm^{-1} (Table S8). These values fall within the anticipated range for a Ni^{II} ion in a distorted octahedral shape [20, 60, 61].

Using the POLY_ANISO program, the exchange-coupled states were developed by considering the total exchange interactions between the Dy–Ni and Ni–Ni ions. The presence of magnetic dipolar interactions ($J_{dipolar}$) and exchange interactions (J_{exch}) have been considered to account for the total magnetic interaction. The latter was included in the Lines model framework [62], and the following equation is used to extract the total exchange interaction:

$$J_{tot} = J_{dipolar} + J_{exch}$$

A satisfactory fit (solid lines) to both susceptibility and magnetization data (Figures 3 and S3) was obtained with the exchange parameters given below. This supports the level of theory used for the calculations [63]. The total exchange interaction (J_{tot}) of the Dy^{III}–Ni^{II} is computed to be −0.61 cm^{-1}, whereas the intra (J_2) and interdimer (J_3) Ni^{II}–Ni^{II} interactions are calculated to be +13.40(2) and −0.05(2) cm^{-1}. It was necessary to include a small intermolecular interaction (*zJ*) with a value of −0.001 cm^{-1}. The major contribution to J_{tot} of Dy^{III}–Ni^{II} thus arises from the dipolar interaction, which is found to be −0.60(2) cm^{-1}, whereas the J_{exch} is only −0.01(2) cm^{-1}. For the Ni^{II}–Ni^{II} intradimer interaction (J_2), the major contribution arises from super exchange, which is found to be +18.4(2) cm^{-1}, whereas the dipolar interaction is −5.0(2) cm^{-1}. In **1**, the two Ni…Ni ions are separated by only 2.902 Å and are bridged by phenoxido groups. In principle, the magnetic dipole–dipole interaction scales as $1/r^3$, such a short metal–metal distance significantly enhances the exchange interaction via through-space dipolar coupling [30–32]. It was previously observed that strong dipolar interactions can be responsible for the manifold of low-lying magnetic states and the observation of any slow relaxation of magnetization in **1** [6, 64]. To verify this further, the *XT* versus T data and magnetization data were simulated with and without including the dipolar coupling. It is clear that the inclusion of the dipolar interactions provides a much better fit to the experimental *XT* and magnetization data (Figures 3 and S3). This confirms that the magnetic properties are strongly dependent on the dipolar exchange interactions [62, 65].

Figure 7 shows the exchange-coupled states computed using POLY_ANISO, which predicts that **1** is unlikely to show SMM behavior given its large tunneling gap in the ground state, which allows for fast relaxation (Table S9). As we go to the excited states, the tunneling gap started increasing, and it dropped to a lower value at the ninth to tenth excited states, giving an energy

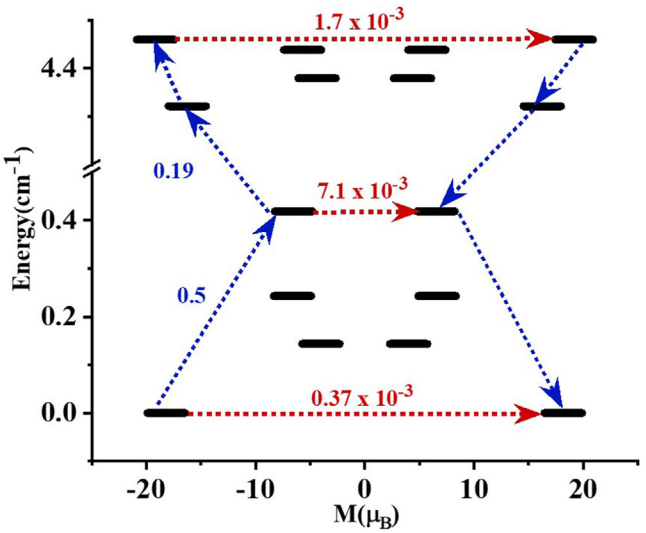

FIGURE 7 | Low-lying exchange spectrum for **1**. The exchange-coupled states are placed on the diagram according to their magnetic moments (bold black lines). The blue arrows show the possible pathway via Orbach/Raman relaxation. The solid red lines represent the tunneling gap (Δ_{tun}) between the doublet states.

barrier of 9.16 cm^{-1} (13.2 K). This prediction is in good agreement with the lack of maxima in the out-of-phase component of the ac susceptibility (Figure S5) under a zero-dc field, but the field-induced SMM behavior with a U_{eff} of 18.3 K for complex **1**. The importance of Ni–Ni and Dy–Ni interactions (mainly due to dipolar coupling) has been further verified by developing the exchange-coupled state diagram by considering only the Dy–Dy interactions, which yielded a negligible energy barrier (Figure S15). This further confirms the significance of Ni–Ni and Dy–Ni dipolar interactions in the SMM behavior of these complexes.

3 | Conclusion

In conclusion, we have synthesized a carbonate-containing dodecanuclear Ni_8Dy_4 (**1**) coordination cluster and its Gd (**2**) and Y (**3**) analogs. DFT methods were performed on the isostructural complexes **2** and **3** to compute Gd^{III}–Ni^{II} and Ni^{II}–Ni^{II} interactions. We investigated the spin structure of **1** using quantum chemical methods (*ab initio* CASSCF, SINGLE_ANISO, and POLY_ANISO). We obtained a spin structure with competing Ni–Dy as well as intra- and interdimer Ni–Ni interactions. This demonstrates how the transition metal ions steer the spin arrangement of this heterometallic 3d–4f cluster. We used the calculations to rationalize the low temperature magnetic behavior revealed by microSQUID measurements. Furthermore, we could show the importance of dipolar interactions to simulate the experimental magnetic dc data and their importance in terms of the SMM characteristics of **1**.

Acknowledgments

The authors are grateful to the DFG Center for Functional Nanostructures for financial support. I.J.D. thanks the DST-INSPIRE (IF220060) for providing a PhD fellowship and DAAD for the exchange program fellowship. K.R.V. thanks the IISER Mohali-High Performing Computing (IISERM-HPC) facility and Prof. Gopalan Rajaraman, IIT Bombay, for providing computing resources. K.R.V. also thanks SERB for providing start-up research grant funding (SRG/2023/000286). J.B., W.W., C.E.A., and A.K.P. thank the DFG CRC1573 "4f for Future" and the Helmholtz Association POF MSE for funding.

Open access funding enabled and organized by Projekt DEAL.

Funding

This study was supported by the Deutsche Forschungsgemeinschaft.

Conflicts of Interest

The authors declare no conflicts of interest.

Data Availability Statement

The data that support the findings of this study are openly available in CCDC at https://www.ccdc.cam.ac.uk/structures/, reference number 2555790.

References

1. J. Tang, I. Hewitt, N. T. Madhu, et al., "Dysprosium Triangles Showing Single-Molecule Magnet Behavior of Thermally Excited Spin States," *Angewandte Chemie International Edition* 45 (2006): 1729–1733, https://doi.org/10.1002/anie.200503564.

2. Y.-N. Guo, G.-F. Xu, W. Wernsdorfer, et al., "Strong Axiality and Ising Exchange Interaction Suppress Zero-Field Tunneling of Magnetization of an Asymmetric Dy_2 Single-Molecule Magnet," *Journal of the American Chemical Society* 133 (2011): 11948–11951, https://doi.org/10.1021/ja205035g.

3. M. Gysler, F. El Hallak, L. Ungur, et al., "Multitechnique Investigation of Dy_3—Implications for Coupled Lanthanide Clusters," *Chemical Science* 7 (2016): 4347–4354, https://doi.org/10.1039/C6SC00318D.

4. Y. Peng, J. Braun, L. Scherthan, et al., "Adding ^{161}Dy-Mössbauer Spectroscopy to a Multitechnique Investigation of Magnetic Transitions in a $\{Co^{III}_3Dy^{III}_3\}$ Single-Molecule Toroic," *Nature Communications* 17 (2026): 3864.

5. Y. Peng, J. Braun, M. Schulze, et al., "A Nested Spin Structure and Single Molecule Magnet Behaviour in an Fe_8 Dy_{12} Heterometallic Cyclic Coordination Cluster," *Dalton Transactions* 53 (2024): 894–897, https://doi.org/10.1039/D3DT04141G.

6. H. Kaemmerer, A. Baniodeh, Y. Peng, et al., "Inorganic Approach to Stabilizing Nanoscale Toroidicity in a Tetraicosanuclear Fe_{18} Dy_6 Single Molecule Magnet," *Journal of the American Chemical Society* 142 (2020): 14838–14842, https://doi.org/10.1021/jacs.0c07168.

7. H.-L. Zhang, Y.-Q. Zhai, L. Qin, L. Ungur, H. Nojiri, and Y.-Z. Zheng, "Single-Molecule Toroic Design Through Magnetic Exchange Coupling," *Matter* 2 (2020): 1481–1493, https://doi.org/10.1016/j.matt.2020.02.021.

8. K. R. Vignesh, S. K. Langley, B. Moubaraki, K. S. Murray, and G. Rajaraman, "Large Hexadecametallic $\{Mn^{III}$–$Ln^{III}\}$ Wheels: Synthesis, Structural, Magnetic, and Theoretical Characterization," *Chemistry—A European Journal* 21 (2015): 16364–16369, https://doi.org/10.1002/chem.201503424.

9. L. Qin, J. Singleton, W. P. Chen, et al., "Quantum Monte Carlo Simulations and High-Field Magnetization Studies of Antiferromagnetic Interactions in a Giant Hetero-Spin Ring," *Angewandte Chemie International Edition* 56 (2017): 16571–16574, https://doi.org/10.1002/anie.201709650.

10. G. A. Craig and M. Murrie, "3d Single-Ion Magnets," *Chemical Society Reviews* 44 (2015): 2135–2147, https://doi.org/10.1039/C4CS00439F.

11. M. Feng and M. L. Tong, "Single Ion Magnets From 3d to 5f: Developments and Strategies," *Chemistry—A European Journal* 24 (2018): 7574–7594, https://doi.org/10.1002/chem.201705761.

12. K. A. Schulte, K. R. Vignesh, and K. R. Dunbar, "Effects of Coordination Sphere on Unusually Large Zero Field Splitting and Slow Magnetic Relaxation in Trigonally Symmetric Molecules," *Chemical Science* 9 (2018): 9018–9026, https://doi.org/10.1039/C8SC02820F.

13. M. A. Hay, A. Sarkar, G. A. Craig, et al., "In-Depth Investigation of Large Axial Magnetic Anisotropy in Monometallic 3d Complexes Using Frequency Domain Magnetic Resonance and Ab Initio Methods: A Study of Trigonal Bipyramidal Co(ii)," *Chemical Science* 10 (2019): 6354–6361, https://doi.org/10.1039/C9SC00987F.

14. G. A. Craig, A. Sarkar, C. H. Woodall, et al., "Probing the Origin of the Giant Magnetic Anisotropy in Trigonal Bipyramidal Ni(ii) Under High Pressure," *Chemical Science* 9 (2018): 1551–1559, https://doi.org/10.1039/C7SC04460G.

15. J. M. Frost, K. L. M. Harriman, and M. Murugesu, "The Rise of 3-d Single-Ion Magnets in Molecular Magnetism: Towards Materials From Molecules?" *Chemical Science* 7 (2016): 2470–2491, https://doi.org/10.1039/C5SC03224E.

16. K. E. R. Marriott, L. Bhaskaran, C. Wilson, et al., "Pushing the Limits of Magnetic Anisotropy in Trigonal Bipyramidal Ni(ii)," *Chemical Science* 6 (2015): 6823–6828, https://doi.org/10.1039/C5SC02854J.

17. A. Chakraborty, J. Goura, P. Bag, and V. Chandrasekhar, "Ni^{II}-Ln^{III} Heterometallic Complexes as Single-Molecule Magnets," *European Journal of Inorganic Chemistry* 2019 (2019): 1180–1200, https://doi.org/10.1002/ejic.201801428.

18. G. Rogez, J.-N. Rebilly, A.-L. Barra, et al., "Very Large Ising-Type Magnetic Anisotropy in a Mononuclear Ni^{II} Complex," *Angewandte Chemie International Edition* 44 (2005): 1876–1879, https://doi.org/10.1002/anie.200462294.

19. A. Upadhyay, N. Komatireddy, A. Ghirri, et al., "Synthesis and Magnetothermal Properties of a Ferromagnetically Coupled Ni^{II}–Gd^{III}–Ni^{II} Cluster," *Dalton Transactions* 43 (2014): 259–266, https://doi.org/10.1039/C3DT52384E.

20. S. K. Singh, N. K. Tibrewal, and G. Rajaraman, "Density Functional Studies on Dinuclear {NiIIGdIII} and Trinuclear {NiIIGdIIINiII} Complexes: Magnetic Exchange and Magneto-Structural Maps," *Dalton Transactions* 40 (2011): 10897, https://doi.org/10.1039/c1dt10600g.

21. J.-P. Costes, T. Yamaguchi, M. Kojima, and L. Vendier, "Experimental Evidence for the Participation of 5d Gd^{III} Orbitals in the Magnetic Interaction in Ni−Gd Complexes," *Inorganic Chemistry* 48 (2009): 5555–5561, https://doi.org/10.1021/ic900142h.

22. V. Chandrasekhar, B. M. Pandian, R. Boomishankar, et al., "Trinuclear Heterobimetallic Ni_2 Ln Complexes $[L_2Ni_2Ln][ClO_4]$ (Ln = La, Ce, Pr, Nd, Sm, Eu, Gd, Tb, Dy, Ho, and Er; LH_3 = (S)P[N(Me)N═CH−C_6 H_3—2 -OH-3 -OMe]$_3$): From Simple Paramagnetic Complexes to Single-Molecule Magnet Behavior," *Inorganic Chemistry* 47 (2008): 4918–4929, https://doi.org/10.1021/ic800199x.

23. N. Ahmed, C. Das, S. Vaidya, S. K. Langley, K. S. Murray, and M. Shanmugam, "Nickel(II)–Lanthanide(III) Magnetic Exchange Coupling Influencing Single-Molecule Magnetic Features in {Ni_2 Ln_2} Complexes," *Chemistry—A European Journal* 20 (2014): 14235–14239, https://doi.org/10.1002/chem.201404393.

24. V. Chandrasekhar, P. Bag, W. Kroener, K. Gieb, and P. Müller, "Pentanuclear Heterometallic {Ni_2 Ln_3} (Ln = Gd, Dy, Tb, Ho) Assemblies. Single-Molecule Magnet Behavior and Multistep Relaxation in the Dysprosium Derivative," *Inorganic Chemistry* 52 (2013): 13078–13086, https://doi.org/10.1021/ic4019025.

25. K. C. Mondal, G. E. Kostakis, Y. Lan, W. Wernsdorfer, C. E. Anson, and A. K. Powell, "Defect-Dicubane Ni_2 Ln_2 (Ln = Dy, Tb) Single Molecule Magnets," *Inorganic Chemistry* 50 (2011): 11604–11611, https://doi.org/10.1021/ic2015397.

26. J. Goura, R. Guillaume, E. Rivière, and V. Chandrasekhar, "Hexanuclear, Heterometallic, Ni_3 Ln_3 Complexes Possessing O-Capped Homo- and Heterometallic Structural Subunits: SMM Behavior of the Dysprosium Analogue," *Inorganic Chemistry* 53 (2014): 7815–7823, https://doi.org/10.1021/ic403090z.

27. S. Maity, T. K. Ghosh, C. J. Gómez-García, and A. Ghosh, "Hexanuclear Ni^{I}_4 Ln^{II}_2 Complexes With SMM Behavior at Zero Field for Ln = Tb, Dy, Ho," *Crystal Growth & Design* 20 (2020): 7300–7311, https://doi.org/10.1021/acs.cgd.0c00957.

28. G. J. Zhou, W. P. Chen, Y. Yu, L. Qin, T. Han, and Y. Z. Zheng, "Filling the Missing Links of M $_{3n}$ Prototype 3d-4f and 4f Cyclic Coordination Cages: Syntheses, Structures, and Magnetic Properties of the Ni_{10} Ln_5 and the Er $_{3n}$ Wheels," *Inorganic Chemistry* 56 (2017): 12821–12829, https://doi.org/10.1021/acs.inorgchem.7b01569.

29. Z. Lu, Z. Zhuo, W. Wang, Y.-G. Huang, and M. Hong, "{Gd_{44} Ni_{22}}: A Gigantic 3d–4f Wheel-Like Nanoscale Cluster With a Large Magnetocaloric Effect," *Inorganic Chemistry Frontiers* 10 (2023): 979–983, https://doi.org/10.1039/D2QI02294J.

30. J. Xi, A.-Z. Huang, Y.-F. Deng, Y.-Q. Zhang, and Y.-Z. Zhang, "Tetrazine-Radical-Bridged Lanthanide Complexes: From Di- to Trinuclear Single-Molecule Magnets," *Inorganic Chemistry* 65 (2026): 1900–1910, https://doi.org/10.1021/acs.inorgchem.5c04614.

31. Y.-H. Qin, X.-F. Ma, X. Hou, et al., "Photoresponsive Luminescent Single-Molecule Magnets Based on Dysprosium–Anthracene Complexes: Regulating the De-Dimerization Temperature of the Photocycloaddition Product by Co-Ligand," *Chemical Science* 16 (2025): 19806–19819, https://doi.org/10.1039/D5SC04192A.

32. B. S. Dolinar, D. I. Alexandropoulos, K. R. Vignesh, T. A. James, and K. R. Dunbar, "Lanthanide Triangles Supported by Radical Bridging Ligands," *Journal of the American Chemical Society* 140 (2018): 908–911, https://doi.org/10.1021/jacs.7b12495.

33. A. A. Lozano, M. Saez, J. Perez, et al., *Dalton Transactions* 35 (2006): 3906–3911.

34. H. Tian, Y. N. Guo, L. Zhao, J. Tang, and Z. Liu, "Hexanuclear Dysprosium(III) Compound Incorporating Vertex- and Edge-Sharing Dy_3 Triangles Exhibiting Single-Molecule-Magnet Behavior," *Inorganic Chemistry* 50 (2011): 8688–8690, https://doi.org/10.1021/ic201121p.

35. H. Ke, L. Zhao, G. F. Xu, et al., "Templated Assembly of μ_5-CO_{32}−Decanuclear Praseodymium and Neodymium Clusters Through Spontaneous Fixation of Atmospheric Carbon Dioxide," *Dalton Transactions* 38 (2009): 10609–10613, https://doi.org/10.1039/b918772c.

36. X.-J. Kong, Y.-P. Ren, L.-S. Long, et al., "Dual Shell-Like Magnetic Clusters Containing Ni^{II} and Ln^{III} (Ln = La, Pr, and Nd) Ions," *Inorganic Chemistry* 47 (2008): 2728–2739, https://doi.org/10.1021/ic702079e.

37. K. K. Nanda, L. K. Thompson, J. N. Bridson, and K. Nag, "Linear Dependence of Spin Exchange Coupling Constant on Bridge Angle in Phenoxy-Bridged Dinickel(II) Complexes," *Journal of the Chemical Society, Chemical Communications* 30 (1994): 1337–1338, https://doi.org/10.1039/c39940001337.

38. C. Benelli and D. Gatteschi, "Magnetism of Lanthanides in Molecular Materials With Transition-Metal Ions and Organic Radicals," *Chemical Reviews* 102 (2002): 2369–2388, https://doi.org/10.1021/cr010303r.

39. A. M. Ako, V. Mereacre, I. J. Hewitt, et al., "Enhancing Single Molecule Magnet Parameters. Synthesis, Crystal Structures and Magnetic Properties of Mixed-Valent Mn_4 SMMs," *Journal of Materials Chemistry* 16 (2006): 2579–2586, https://doi.org/10.1039/B604611H.

40. F. Pointillart, K. Bernot, R. Sessoli, and D. Gatteschi, "Effects of 3d–4f Magnetic Exchange Interactions on the Dynamics of the Magnetization of Dy^{III}-M^{II}-Dy^{III} Trinuclear Clusters," *Chemistry—A European Journal* 13 (2007): 1602–1609, https://doi.org/10.1002/chem.200601194.

41. G. Novitchi, W. Wernsdorfer, L. F. Chibotaru, J. P. Costes, C. E. Anson, and A. K. Powell, "Supramolecular "Double-Propeller" Dimers of Hexanuclear Cu^{II}/Ln^{III} Complexes: A {Cu_3Dy_3}$_2$ Single-Molecule Magnet," *Angewandte Chemie International Edition* 48 (2009): 1614–1619, https://doi.org/10.1002/anie.200805176.

42. D. Schray, G. Abbas, Y. Lan, et al., "Combined Magnetic Susceptibility Measurements and[57] Fe Mössbauer Spectroscopy on a Ferromagnetic {$Fe^{II}_4Dy_4$} Ring," *Angewandte Chemie International Edition* 49 (2010): 5185–5188, https://doi.org/10.1002/anie.201001110.

43. M. Hołyńska, D. Premužić, I.-R. Jeon, W. Wernsdorfer, R. Clérac, and S. Dehnen, "[Mn^{II}_6 O_3 Ln_2] Single-Molecule Magnets: Increasing the Energy Barrier Above 100 K," *Chemistry—A European Journal* 17 (2011): 9605–9610, https://doi.org/10.1002/chem.201101807.

44. W. Wernsdorfer, "Classical and Quantum Magnetization Reversal Studied in Nanometer-Sized Particles and Clusters," in *Advances in Chemical Physics*, Vol. 118 ed. I. Prigogine and S. A. Rice (2001), https://doi.org/10.1002/9780470141786.ch3.

45. N. F. Chilton, R. P. Anderson, L. D. Turner, A. Soncini, and K. S. Murray, "PHI: A Powerful New Program for the Analysis of Anisotropic Monomeric and Exchange-Coupled Polynuclear d- and f -Block Complexes," *Journal of Computational Chemistry* 34 (2013): 1164–1175, https://doi.org/10.1002/jcc.23234.

46. K. R. Vignesh, S. K. Langley, C. J. Gartshore, B. Moubaraki, K. S. Murray, and G. Rajaraman, "What Controls the Magnetic Exchange and Anisotropy in a Family of Tetranuclear {Mn^{II} Mn^{III} } Single-Molecule Magnets?," *Inorganic Chemistry* 56 (2017): 1932–1949, https://doi.org/10.1021/acs.inorgchem.6b02527.

47. K. R. Vignesh, S. K. Langley, B. Moubaraki, K. S. Murray, and G. Rajaraman, "Understanding the Mechanism of Magnetic Relaxation in Pentanuclear {Mn^{IV} Mn^{II}_2 Ln^{II}_2} Single-Molecule Magnets," *Inorganic Chemistry* 57 (2018): 1158–1170, https://doi.org/10.1021/acs.inorgchem.7b02608.

48. D. Chauhan, K. R. Vignesh, A. Swain, et al., "Exploiting Strong {Cr^{III}–Dy^{III} } Ferromagnetic Exchange Coupling to Quench Quantum Tunneling of Magnetization in a Novel {Cr^{II}_2 Dy^{II}_3} Single-Molecule Magnet," *Crystal Growth & Design* 23 (2022): 197–206, https://doi.org/10.1021/acs.cgd.2c00888.

49. G. A. Craig, G. Velmurugan, C. Wilson, R. Valiente, G. Rajaraman, and M. Murrie, "Magnetic Properties of a Family of [Mn^{II}_4 Ln^{II}_4] Wheel Complexes: An Experimental and Theoretical Study," *Inorganic Chemistry* 58 (2019): 13815–13825, https://doi.org/10.1021/acs.inorgchem.9b01592.

50. I. J. Dutta, V. Kasi, D. Chauhan, et al., "Quenching Quantum Tunnelling of the Magnetization Utilizing 4d–4f Exchange Interactions in Butterfly-Shaped {RuIII2LnIII2} (Ln = Gd, Tb, Dy, Ho, and Er) Single-Molecule Magnets," *Inorganic Chemistry Frontiers* 13 (2026): 138–154, https://doi.org/10.1039/D5QI01665G.

51. X. J. Kong, Y. P. Ren, W. X. Chen, et al., "A Four-Shell, Nesting Doll-Like 3d–4f Cluster Containing 108 Metal Ions," *Angewandte Chemie International Edition* 47 (2008): 2398–2401, https://doi.org/10.1002/anie.200705731.

52. J. B. Peng, Q. C. Zhang, X. J. Kong, et al., "High-Nuclearity 3d–4f Clusters as Enhanced Magnetic Coolers and Molecular Magnets," *Journal of the American Chemical Society* 134 (2012): 3314–3317, https://doi.org/10.1021/ja209752z.

53. W. P. Chen, P. Q. Liao, Y. Yu, Z. Zheng, X. M. Chen, and Y. Z. Zheng, "A Mixed-Ligand Approach for a Gigantic and Hollow Heterometallic Cage {Ni_{64} RE_{96}} for Gas Separation and Magnetic Cooling Applications," *Angewandte Chemie International Edition* 55 (2016): 9375–9379, https://doi.org/10.1002/anie.201603907.

54. D. P. Liu, X. P. Lin, H. Zhang, et al., "Magnetic Properties of a Single-Molecule Lanthanide–Transition-Metal Compound Containing 52 Gadolinium and 56 Nickel Atoms," *Angewandte Chemie International Edition* 55 (2016): 4532–4536, https://doi.org/10.1002/anie.201601199.

55. Q. F. Lin, J. Li, X. M. Luo, C. H. Cui, Y. Song, and Y. Xu, "Incorporation of Silicon–Oxygen Tetrahedron Into Novel High-Nuclearity Nanosized 3d–4f Heterometallic Clusters," *Inorganic Chemistry* 57 (2018): 4799–4802, https://doi.org/10.1021/acs.inorgchem.8b00327.

56. W. P. Chen, P. Q. Liao, P. B. Jin, et al., "The Gigantic {Ni_{36} Gd_{102}} Hexagon: A Sulfate-Templated "Star-of-David" for Photocatalytic CO_2 Reduction and Magnetic Cooling," *Journal of the American Chemical Society* 142 (2020): 4663–4670, https://doi.org/10.1021/jacs.9b11543.

57. A. Bhanja, L. Smythe, R. Herchel, I. Nemec, M. Murrie, and D. Ray, "Hydroxido Supported and Differently Networked Octanuclear Ni_6 Ln_2 [Ln = Gd^{III} and Dy^{III}] Complexes: Structural Variation, Magnetic Properties and Theoretical Insights," *Dalton Transactions* 50 (2021): 5023–5035, https://doi.org/10.1039/D0DT04168H.

58. F. Aquilante, J. Autschbach, R. K. Carlson, et al., "Molcas 8: New Capabilities for Multiconfigurational Quantum Chemical Calculations Across the Periodic Table," *Journal of Computational Chemistry* 37 (2016): 506–541, https://doi.org/10.1002/jcc.24221.

59. K. R. Vignesh, S. K. Langley, K. S. Murray, and G. Rajaraman, "Exploring the Influence of Diamagnetic Ions on the Mechanism of Magnetization Relaxation in {Co^{II}_2 Ln^{II}_2} (Ln = Dy, Tb, Ho) "Butterfly" Complexes," *Inorganic Chemistry* 56 (2017): 2518–2532, https://doi.org/10.1021/acs.inorgchem.6b02720.

60. S. Sasmal, S. Hazra, P. Kundu, et al., "Magnetic Exchange Interactions and Magneto-Structural Correlations in Heterobridged μ-Phenoxo-$\mu_{1,1}$-Azide Dinickel(II) Compounds: A Combined Experimental and Theoretical Exploration," *Inorganic Chemistry* 50 (2011): 7257–7267, https://doi.org/10.1021/ic200833y.

61. P. Comba, M. Enders, M. Großhauser, et al., "Validation of Ab-Initio-Predicted Magnetic Anisotropies and Magneto-Structural Correlations in Linear Hetero-Trinuclear Dy^{III} -Ni^{I}_2 Compounds," *Chemistry—A European Journal* 27 (2021): 9372–9382, https://doi.org/10.1002/chem.202100626.

62. M. E. Lines, "Orbital Angular Momentum in the Theory of Paramagnetic Clusters," *Journal of Chemical Physics* 55 (1971): 2977–2984, https://doi.org/10.1063/1.1676524.

63. G. Fernandez Garcia, D. Guettas, V. Montigaud, et al., "A Dy_4 Cubane: A New Member in the Single-Molecule Toroics Family," *Angewandte Chemie International Edition* 57 (2018): 17089–17093, https://doi.org/10.1002/anie.201810156.

64. K. R. Vignesh, S. K. Langley, A. Swain, et al., "Slow Magnetic Relaxation and Single-Molecule Toroidal Behaviour in a Family of Heptanuclear {Cr^{III} Ln^{II}_6} (Ln=Tb, Ho, Er) Complexes," *Angewandte Chemie International Edition* 57 (2018): 779–784, https://doi.org/10.1002/anie.201711844.

65. K. R. Vignesh, A. Soncini, S. K. Langley, W. Wernsdorfer, K. S. Murray, and G. Rajaraman, "Ferrotoroidic Ground State in a Heterometallic {CrIIIDyIII 6} Complex Displaying Slow Magnetic Relaxation," *Nature Communications* 8 (2017): 1023, https://doi.org/10.1038/s41467-017-01102-5.

66. L. Noodleman, "Valence Bond Description of Antiferromagnetic Coupling in Transition Metal Dimers," *Journal of Chemical Physics* 74 (1981): 5737–5743, https://doi.org/10.1063/1.440939.

67. A. D. Becke, "Density-Functional Thermochemistry. III. The Role of Exact Exchange," *Journal of Chemical Physics* 98 (1993): 5648–5652, https://doi.org/10.1063/1.464913.

68. T. R. Cundari and W. J. Stevens, "Effective Core Potential Methods for the Lanthanides," *Journal of Chemical Physics* 98 (1993): 5555–5565, https://doi.org/10.1063/1.464902.

69. B. A. Heß, C. M. Marian, U. Wahlgren, and O. Gropen, "A Mean-Field Spin-Orbit Method Applicable to Correlated Wavefunctions," *Chemical Physics Letters* 251 (1996): 365–371, https://doi.org/10.1016/0009-2614(96)00119-4.

70. P. Å. Malmqvist, B. O. Roos, and B. Schimmelpfennig, "The Restricted Active Space (RAS) State Interaction Approach With Spin–Orbit Coupling," *Chemical Physics Letters* 357 (2002): 230–240, https://doi.org/10.1016/S0009-2614(02)00498-0.

71. B. O. Roos and P.-A. Malmqvist, "Relativistic Quantum Chemistry: The Multiconfigurational Approach," *Physical Chemistry Chemical Physics* 6 (2004): 2919, https://doi.org/10.1039/b401472n.

72. B. O. Roos, R. Lindh, P. A. Malmqvist, V. Veryazov, P. O. Widmark, and A. C. Borin, "New Relativistic Atomic Natural Orbital Basis Sets for Lanthanide Atoms With Applications to the Ce Diatom and LuF_3," *Journal of Physical Chemistry A* 112 (2008): 11431–11435, https://doi.org/10.1021/jp803213j.

73. G. M. Sheldrick, "A Short History of SHELX," *Acta Crystallographica Section A Foundations of Crystallography* 64 (2008): 112–122, https://doi.org/10.1107/S0108767307043930.

74. L. F. Chibotaru and L. Ungur, "Ab Initio Calculation of Anisotropic Magnetic Properties of Complexes. I. Unique Definition of Pseudospin Hamiltonians and Their Derivation," *Journal of Chemical Physics* 137 (2012): 064112, https://doi.org/10.1063/1.4739763.

75. L. J. Bourhis, O. V. Dolomanov, R. J. Gildea, J. A. Howard, and H. Puschmann, "The Anatomy of a Comprehensive Constrained, Restrained Refinement Program for the Modern Computing Environment—$Olex_2$ Dissected," *Acta Crystallographica Section A Foundations and Advances* 71 (2015): 59–75, https://doi.org/10.1107/S2053273314022207.

76. G. M. Sheldrick, "Crystal Structure Refinement With SHELXL," *Acta Crystallographica Section C Structural Chemistry* 71 (2015): 3–8, https://doi.org/10.1107/S2053229614024218.

77. A. L. Spek, "PLATON SQUEEZE: A Tool for the Calculation of the Disordered Solvent Contribution to the Calculated Structure Factors," *Acta Crystallographica Section C Structural Chemistry* 71 (2015): 9–18, https://doi.org/10.1107/S2053229614024929.

78. M. J. Frisch, G. W. Trucks, H. B. Schlegel, et al., Wallingford, CT, (2016).

79. F. Neese, "Software Update: The ORCA Program System—Version 5.0," *Wiley Interdisciplinary Reviews: Computational Molecular Science* 12 (2022): e1606, https://doi.org/10.1002/wcms.1606.

Supporting Information

Additional supporting information can be found online in the Supporting Information section.

The authors have cited additional references within the Supporting Information [66–79]. Full crystallographic data and details of the structural determination for (**1**) have been deposited with the Cambridge Crystallographic Data Centre as supplementary publication no. CCDC 2555790. Copies of the data can be obtained, free of charge, from https://www.ccdc.cam.ac.uk/structures/.

Supporting File 1: chem71499-sup-0001-SupMat.docx